Science Bulletin 68 (2023) 3252–3260

Contents lists available at ScienceDirect

Science Bulletin

journal homepage: www.elsevier.com/locate/scib

Review

Measurements of the lightest hypernucleus ($^3_\Lambda$H): progress and perspective

Jinhui Chen [a,b,*], Xin Dong [c,*], Yu-Gang Ma [a,b,*], Zhangbu Xu [d,*]

[a] Key Laboratory of Nuclear Physics and Ion-beam Application (Ministry of Education), Institute of Modern Physics, Fudan University, Shanghai 200433, China
[b] Shanghai Research Center for Theoretical Nuclear Physics, National Natural Science Foundation of China, Fudan University, Shanghai 200438, China
[c] Lawrence Berkeley National Laboratory, Berkeley CA 94720, USA
[d] Brookhaven National Laboratory, Upton NY 11973, USA

ARTICLE INFO

Article history:
Received 16 September 2023
Received in revised form 25 October 2023
Accepted 16 November 2023
Available online 23 November 2023

Keywords:
Heavy-ion collisions
Hyperon-nucleon interaction
Hypernuclei

ABSTRACT

The hyperon-nucleon (Y-N) interaction is important for the description of the equation-of-state of high baryon density matter. Hypernuclei, the cluster object of nucleons and hyperons, serve as cornerstones of a full understanding of the Y-N interaction. Recent measurements of the lightest known hypernucleus, the hypertriton's ($^3_\Lambda$H) and anti-hypertriton's ($^3_\Lambda\bar{\text{H}}$) lifetime, mass and Λ separation energy have attracted interests on the subject. Its cross section and collective flow parameters have also been measured in heavy-ion collisions, which have revealed new features on its production mechanism. In this article we summarise recent measurements of $^3_\Lambda$H, focusing on the heavy-ion collisions. We will discuss their implications for the $^3_\Lambda$H properties and the constrains on the Y-N interaction models.

1. Introduction

Although the structure of nuclei in nature is determined by the strong force that bind neutrons and protons into the clusters, and we have a good understanding of the quantum chromodynamics (QCD) theory at the fundamental level [1,2], the theory itself is not always directly applicable to nuclear structure. It remains one of the scientific quests on whether the fundamental interactions that are basic to the structure of matter could be fully understood [3]. As the energy scale increases in nuclear reactions and/or the energy density increases in stars, strangeness quantum number may come into play [4]. Hypernuclei are bound state of normal nuclei with an additional strange baryon, such as Λ, Σ, Ξ and Ω hyperons. Such nuclear objects have been the natural tool to study the hyperon-nucleon (Y-N) interaction since the discovery of the first element [5] exactly seven decades ago. The Y-N interaction is theoretically predicted to be the important ingredient to describe the equation-of-state of astrophysical objects such as neutron stars [6,7], which, depending on the strength of the interaction, might be a hyperon star, might be composed of strange quark matter, or might have a kaon condensate at its core [6]. Because hyperons are not stable in the vacuum, it is challenging to operate direct hyperon-nucleon scattering experiments in the way of electron scattering to probe the nuclei structure. To date, hypernucleus still represents a practical laboratory ideal for studying the Y-N interaction [8,9].

The lowest mass bound hypernucleus is the hypertriton ($^3_\Lambda$H), which consists of a Λ, a proton and a neutron. It is the most copiously produced hypernucleus in heavy-ion reaction, where is the main scope of current paper. By colliding heavy nuclei at relativistic energies scientists are able to test the nature of nuclear matter at high temperature and density, to produce conditions similar to those thought prevalent in the early universe, and to search for previously unstudied states of nuclear matter [10]. Relativistic heavy-ion collisions create a hot and dense phase of matter containing approximately equal number of quarks and antiquarks, where they are free to move throughout the volume of the nuclear collision region. This phase of matter persists for only a few times 10^{-23} s, then cools and transitions into a less excited phase comprised of mesons, and baryons, including the occasional (anti) nucleus or (anti) hypernucleus. Thus these collisions could be used to explore fundamental physics involving nuclei, hypernuclei [11]. With the added strangeness degree of freedom $^3_\Lambda$H is expected to possess different properties from normal nucleus with similar atomic mass number, such as triton or helium. Therefore, measurements of $^3_\Lambda$H binding energy, excitation energies for particle-bound state, spins, lifetimes, and decay branching ratios will allow us to infer the Y-N interaction from the simplest hypernuclear cluster [12].

* Corresponding authors.
E-mail addresses: chenjinhui@fudan.edu.cn (J. Chen), xdong@lbl.gov (X. Dong), mayugang@fudan.edu.cn (Y.-G. Ma), xzb@bnl.gov (Z. Xu).

https://doi.org/10.1016/j.scib.2023.11.045
2095-9273/

2. The lifetime and Λ separation energy of ${}^{3}_{\Lambda}$H: status and progress

2.1. Status in the early days

The Λ separation energy of ${}^{3}_{\Lambda}$H, the B_Λ Λrepresenting the energy needed to remove Λ from the deuteron core of ${}^{3}_{\Lambda}$H, is defined as

$$B_\Lambda \equiv M_{\rm d} + M_\Lambda - M_{^{3}_{\Lambda}{\rm H}}, \quad (1)$$

which is rather small compared to the normal nuclei or heavy hypernuclei [13–15]. Thus it was argued that the Λ is loosely bound outside the deuteron core in the ${}^{3}_{\Lambda}$H [16], as shown in the Fig. 1. For example, taking the frequently cited value of B_Λ = (0.13 ± 0.05) MeV [13] will result in a large separation of the Λ from the deuteron of about 10 fm [17]. Consequence of such structure is that the lifetime of ${}^{3}_{\Lambda}$H, $\tau({}^{3}_{\Lambda}{\rm H})$, should be very close to the free Λ lifetime (τ_Λ), whose value is $\tau_\Lambda = (263.2 \pm 2.0)$ ps [18]. However, measurements of $\tau({}^{3}_{\Lambda}{\rm H})$ using nuclear emulsions and helium bubble chambers showed a large spread of $\tau({}^{3}_{\Lambda}{\rm H})$ value, ranging from $\approx 0.35\tau_\Lambda$ to $1.08\tau_\Lambda$ with very large statistical uncertainty [19–24]. This raised a puzzle in the field and called for more precise measurements of the ${}^{3}_{\Lambda}$H lifetime to clarify the situation [25,26].

2.2. Lifetime measurements in heavy-ion collisions

The technology to measure the $\tau({}^{3}_{\Lambda}{\rm H})$ in heavy-ion collisions is different from those applied in early days. In helium bubble chamber or nuclear emulsion experiments, ${}^{3}_{\Lambda}$H was observed by analyzing the events produced in the interaction of K^- both in flight and at rest with the nuclei of the sensitive layers of visualizing detectors. In heavy-ion collisions, they are measured by detecting their mesonic decay via the topological identification of secondary vertices and the analysis of the invariant mass distributions of decay particles. Taking the ${}^{3}_{\Lambda}$H decays to ^{3}He and π in Relativistic Heavy Ion Collider (RHIC), the Solenoidal Tracker at RHIC (STAR) experiment as an example, the main STAR detectors used to identify the candidate ^{3}He and π are the Time Projection Chamber (TPC) combined with the Time of Flight detector (TOF), by the mean energy loss per unit track length ($\langle {\rm d}E/{\rm d}x\rangle$) in the TPC gas and the speed (β) determined from TOF measurements. The ${}^{3}_{\Lambda}$H is then measured via the invariant mass of ^{3}He and π. With reconstruction of the ${}^{3}_{\Lambda}$H weak decay vertex up to a few cm away from the collision vertex, together with the high precision tracking and particle identification capabilities of the STAR experiment, the invariant mass of each ${}^{3}_{\Lambda}$H candidate is calculated with a good signal to background ratio. Fig. 2a shows such a distribution in Au + Au collisions at $\sqrt{s_{\rm NN}} = 3$ GeV [27]. To improve the signal to background ratio, machine learning techniques have also been applied in the new data analysis. Taking the result of Ref. [15] in Large Hadron Collider (LHC), A Large Ion Collider Experiment (ALICE) as an example where the detector apparatus is similar to the STAR experiment: cut criteria to optimize the signal are performed with a gradient-boosted decision tree classifier (BDT) and trained on a dedicated Monte Carlo simulated event sample [15]. After such trainings, the selection is based on the BDT score, defining a threshold that maximizes the expected signal to background ratio [15]. Fig. 2b shows such a distribution in Pb + Pb collisions at $\sqrt{s_{\rm NN}} = 5.02$ TeV with almost background free mainly due to the excellent performance of the ALICE Inner Tracking System and the TPC detector [15].

To determine the lifetime, the ${}^{3}_{\Lambda}$H yields are analyzed in differential proper decay length intervals according to the equation

$$N(t) = N(0)\exp(-t/\tau), \quad (2)$$

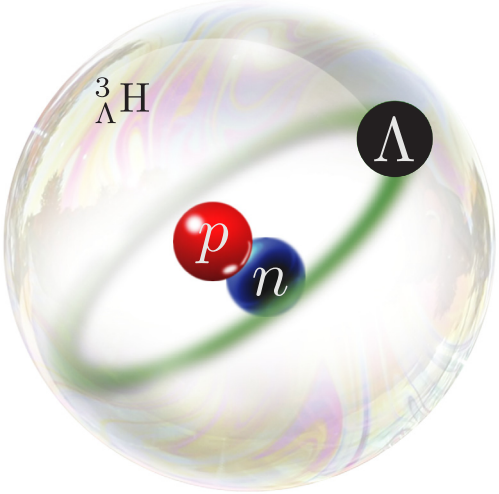

Fig. 1. (Color online) Sketch of the ${}^{3}_{\Lambda}$H structure. Although proton, neutron and Λ by themselves are color neutral, they are painted here by different color for viewing.

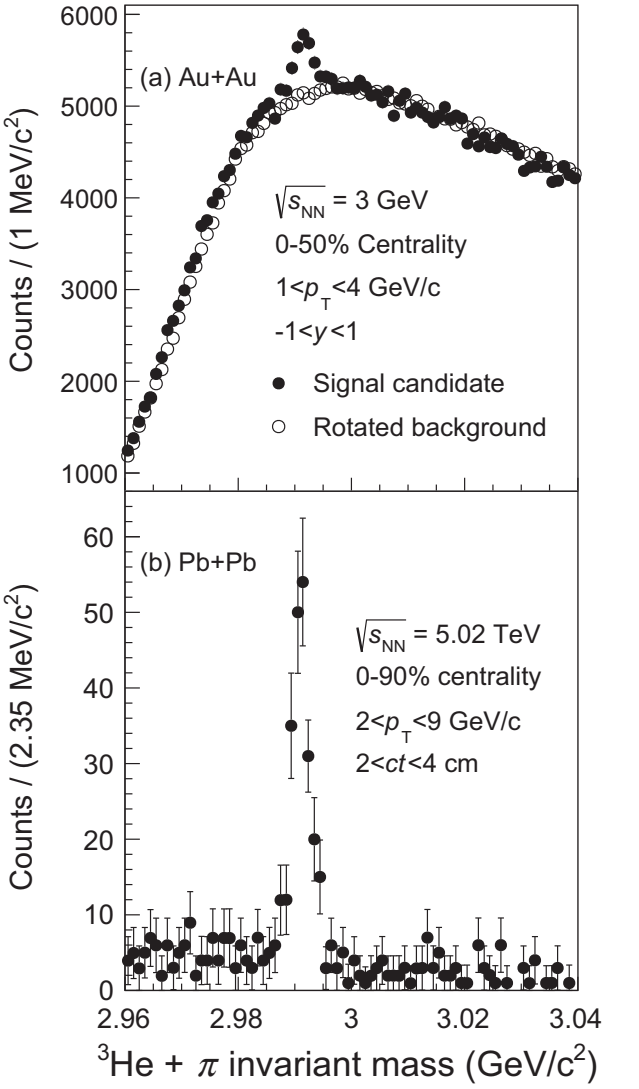

Fig. 2. Invariant mass distributions of ${}^{3}_{\Lambda}$H candidate reconstructed by ^{3}He+π^- with panel (a) from Au + Au collisions at $\sqrt{s_{\rm NN}} = 3$ GeV [27] and panel (b) from Pb + Pb collisions at $\sqrt{s_{\rm NN}} = 5.02$ TeV [15]. Black circles in both panels represent the signal distributions, while open circles in panel (a) are combinatorial background distribution built with rotational daughter track algorithm.

where $t = l/(\beta\gamma c)$, $\beta\gamma c = p/m$, l is the measured decay distance, p is the particle momentum, m is the particle mass, and c is the speed of light. The raw count in different ct bin was extracted from the invariant mass distribution (c.f. Fig. 2). Then the distribution was corrected for the detector acceptance, tracking efficiency and selection efficiency as a function of ct. Fig. 3 shows such distributions in heavy-ion collisions. The lifetime is then extracted by a χ^2 fit of each measurement with the exponential function.

Fig. 4 shows a collection of the world data on $\tau(^3_\Lambda\mathrm{H})$ measurements [15,19–24,27,32]. In comparison with the lifetime of free Λ, the $^3_\Lambda$H data is ranging from ~50% to ~100% of free Λ with considerable uncertainties. An average value of 228.5 ps is obtained by taking the average with $1/(\sigma)^2$ as the weight for each measurement, where σ represents the total experimental uncertainty (statistical and systematical uncertainties added in quadrature if the latter is available). The associated uncertainty on the average value is 11.6 ps, which has been scaled by the $S \equiv \sqrt{\chi^2/(N-1)}$ value of 1.3. Fig. 4 also shows the ideogram distribution, a probability distribution weighted by $1/\sigma$ while σ is the individual experimental data uncertainty. Investigation on the difference between the ideogram curve and measurements may offer information for potentially additional systematics which are not covered by the measurement.

Since measurements in heavy-ion collisions are carried out as a function of proper decay length, it allows for a common fit of the distributions to obtain an average value of $\tau(^3_\Lambda\mathrm{H})$ in heavy-ion collisions. In this analysis, we fit the individual distributions of heavy-ion data simultaneously with a same τ parameter and free normalization parameter for each distribution. The data are described well by the aforementioned exponential function with a probability of 0.2, shown as the red line in Fig. 3. The χ^2 per degree of freedom of 1.22 is slightly larger than unit, which is mainly driven by the data points at lowest ct. We observe that the STAR data point at lowest ct (the open cross) appears to be systematically higher than the exponential function with 2.47σ while the ALICE data point at lowest ct (the open triangle) is lower than the exponential function with 2.10σ. The $\tau(^3_\Lambda\mathrm{H}) = (236.4 \pm 8.1)$ ps is the value from a common fit of data in heavy-ion collisions, where the uncertainty has been scaled by the S value of 1.1. The lifetime of $^3_\Lambda$H from a common fit of heavy-ion collisions data solely is consistent with the average value of world data including early nuclear emulsion measurements and bubble chamber measurements. Our number is ~10% smaller than the value of τ_Λ [18].

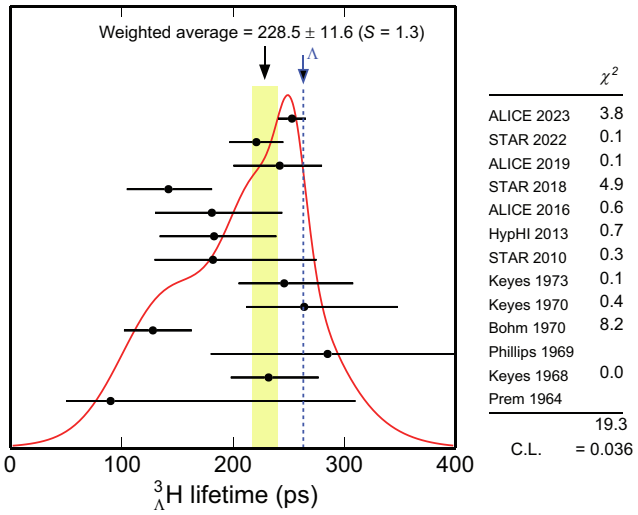

Fig. 4. (Color online) A typical ideogram of the $\tau(^3_\Lambda\mathrm{H})$. The arrow at the top shows the position of the weighted average, while the width of the shaded pattern shows the error in the average after scaling by the factor S. The column on the right gives the χ^2 contribution of each of the experiments. All data are cited in reference [15,19–24,27–32]. The dashed line is the τ_Λ for Ref. [18].

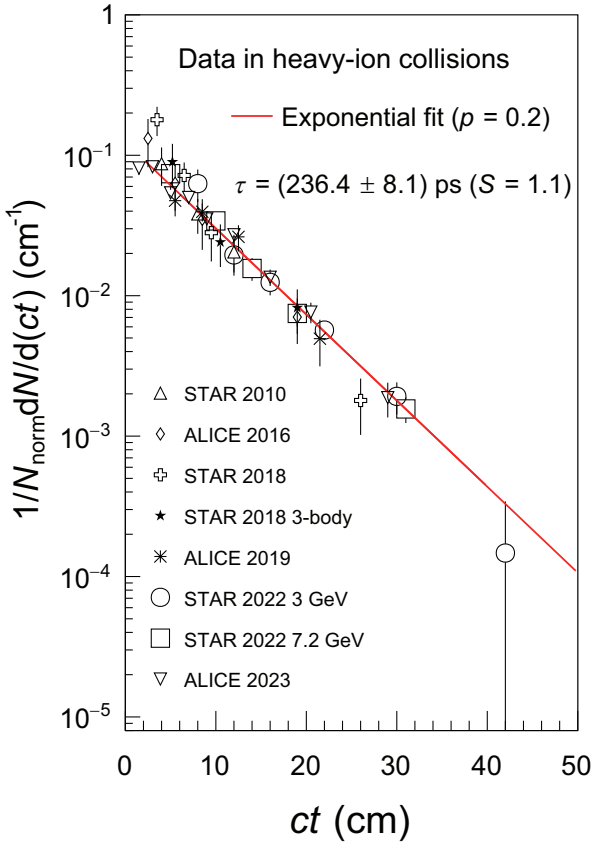

Fig. 3. (Color online) The normalized yield as a function of the proper decay length ct for $^3_\Lambda$H in heavy-ion collisions. The τ parameter of the exponential fit is determined by a common fit to the 8 individual measurements with the same slope parameter, and the associated uncertainty is scaled by S = 1.1. As displayed in the figure, the fit probability (p) is 0.2.

2.3. Λ separation energy

The measurement of B_Λ requires a precise determination of the rest mass of $^3_\Lambda$H. In heavy-ion collisions, $^3_\Lambda$H particle is often reconstructed via its two- or three-body decays involving charged particles by calculating the invariant mass of $^3_\Lambda$H through its decay daughters. The determination of $M(^3_\Lambda\mathrm{H})$ will then require precision momentum calibration of the decay charged daughter tracks. The Λ with a mass of (1115.683 ± 0.006) MeV [18] whose decay has a similar decay topology as the $^3_\Lambda$H decay, therefore is often used to calibrate the experimental momentum distortion correction. Fig. 5 shows one of the mass distributions in Au + Au collisions at $\sqrt{s_{\mathrm{NN}}}$ = 200 GeV by the STAR experiment [14]. Due to the installment of a high-precision tracking detector which was not applied in the Fig. 2a analysis, the invariant mass distributions are reconstructed with a low level of background, which mainly originates from combinatorial contamination and particle misidentification. In the STAR measurement, the invariant mass distributions were then fitted by a Gaussian function plus a linear polynomial using the unbinned maximum likelihood method. The mass parameters are extracted through the peak positions of the invariant mass distributions. An average of mass values from two-body and three-body decay channels weighted by the reciprocal of squared statis-

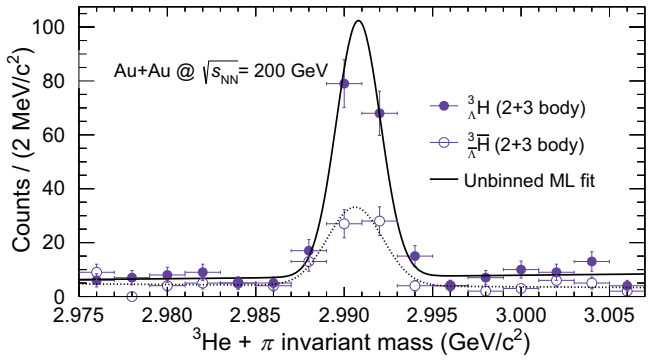

Fig. 5. (Color online) The invariant mass distributions of $^3_\Lambda$H reconstructed via the charged two-body and three-body decay channels $^3_\Lambda\text{H}\to{}^3\text{He}+\pi^-$, $^3_\Lambda\text{H}\to d+p+\pi^-$ and their corresponding charge-conjugated particles $^3_\Lambda\bar{\text{H}}$ in Au + Au collisions at $\sqrt{s_{NN}}$ = 200 GeV by the STAR experiment [14]. Points are data and curves represent a Maximum Likelihood (ML) fit using a Gaussian function plus a linear polynomial for illustration purpose. Mass extraction procedure should be referred to the text of Ref. [14].

tical uncertainties is the final result. One can perform the same average on $^3_\Lambda$H and its antiparticle to improve the precision [14].

Fig. 6 summarizes the experimental measurements of B_Λ of $^3_\Lambda$H from early nuclear emulsion experiments and recent heavy-ion collisions [13–15,23,33,34]. The original data from early experiments have been corrected for the updated M_d and M_Λ since more than half a century ago [35]. The modern heavy-ion experimental data contain both statistical and systematical uncertainties which are added in quadrature in the presented error bars. The yellow band depicts a global average of all data points which yields $B_\Lambda = (0.17 \pm 0.06)$ MeV, where the uncertainty has been scaled by the S = 1.6. Please note that the S value from the average is rather large, indicating a relative large spread of experimental data points.

The red line in Fig. 6 shows the ideogram presentation of the data points which also shows a large spread of the values. Despite the small systematical error assigned to the nuclear emulsion measurements [25], it was shown that for p-shell hypernuclei a discrepancy exists in the range of 400 to 800 keV between nuclear

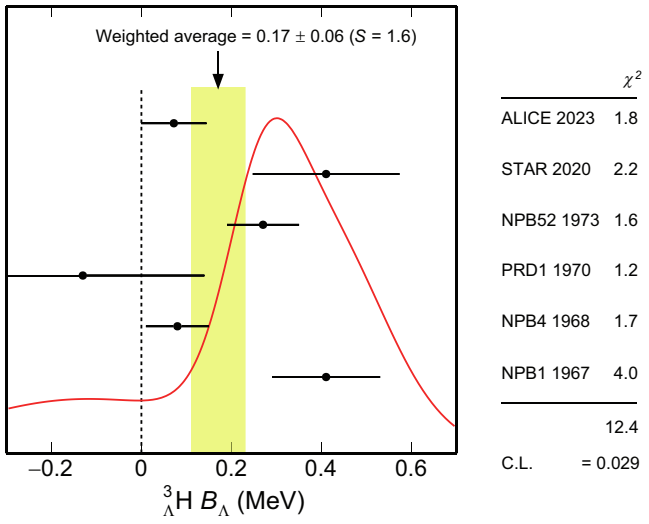

Fig. 6. (Color online) Similar to Fig. 4 but for measurements of the Λ separation energy of $^3_\Lambda$H [33,34,23,13–15]. The arrow at the top shows the position of the weighted average, while the width of the shaded pattern shows the error in the average after scaling by the factor S. The column on the right gives the χ^2 contribution of each of the experiment. The dashed line represents $B_\Lambda = 0$ for reference.

emulsion data [25] and those obtained with (π^+, K^+) reaction [36]. Recalibration of the spectrometer data with respect to different measurements, for example, the data in Ref. [37] reduced the difference, there remained substantial differences between early nuclear emulsion studies and recent spectrometer data with a significant spread of a few hundreds keV for individual hypernuclei. Similar situation is present in the heavy-ion collisions data. A full understanding on the systematics is called for.

Benefit from the excellent resolution of the anti-nuclei mass measurements in high-energy heavy-ion collisions [14,15,38–40], one can measure the mass difference of $^3_\Lambda$H and $^3_\Lambda\bar{\text{H}}$ to probe the matter–antimatter symmetry pertaining to the binding of strange and anti-strange quarks in nuclei. The fundamental symmetry of nature, the CPT theorem which exchanges particles with anti-particles, implies that all physics laws are the same under the simultaneous reversal of charge (C), reflection of spatial coordinates (P) and time inversion (T). Although measurements of mass difference between baryon-antibaryon had reached a very high precision with protons and anti-protons [41], extension the measurement from (anti-) proton to (anti-) nuclei allows one to probe any difference in the interactions between nucleons and anti-nucleons encoded in the (anti-) nuclei masses. This force is a remnant of the underlying strong interaction among quarks and gluons which cannot yet be directly derived from QCD. Fig. 7 shows the mass-over-charge ratio difference, $\frac{\Delta m/|q|}{m/|q|} = \frac{m_A - m_{\bar{A}}}{m_A}$, for d, ^{3}He in Pb + Pb collisions at $\sqrt{s_{NN}} = 2.76$ TeV [38] and $^3_\Lambda$H in Au + Au collisions at $\sqrt{s_{NN}} = 200$ GeV and Pb + Pb collisions at $\sqrt{s_{NN}} = 5.02$ TeV [14,15]. Systematical uncertainties can be reduced by performing mass differences, rather than absolute mass measurements. Within current uncertainties, all data presented in Fig. 7 are consistent with zero, the dashed line in Fig. 7 from CPT invariance expectation. Data from heavy-ion collisions confirm CPT invariance in the sector of light nuclei and light hypernuclei.

3. The yield and collective flow of $^3_\Lambda$H in heavy-ion collisions

Production yields of light nuclei and light hypernuclei are suggested to be related to their internal nuclear structure as well as nucleon-nucleon (N-N) or Y-N interaction [42–44]. To examine the structure and the production mechanism, measurements of $^3_\Lambda$H yield at mid-rapidity (dN/dy) have been performed in Au + Au collisions [27], p + Pb and Pb + Pb collisions [30, 45]. Since the decay branching ratio (B.R.) of $^3_\Lambda\text{H}\to{}^3\text{He}+\pi^-$ was not directly measured, experimental data were presented by the dN/dy times the B.R.. The up panel of Fig. 8 shows the B.R.× dN/dy of $^3_\Lambda$H in Au + Au collisions at $\sqrt{s_{NN}}$ = 3 GeV [27]. To interpret the data, calculations from the transport model, Jet AA Microscopic Trans-

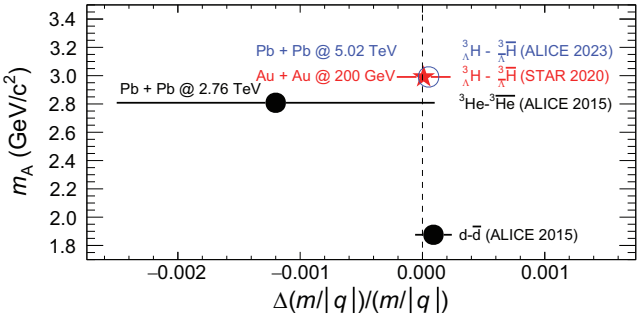

Fig. 7. (Color online) Data [14,15,38] of the mass-over-charge ratio differences for light nuclei and hypernuclei from heavy-ion collisions compared with CPT invariance expectation (dotted line). Error bars represent the sum in quadrature of the statistical and systematical uncertainties.

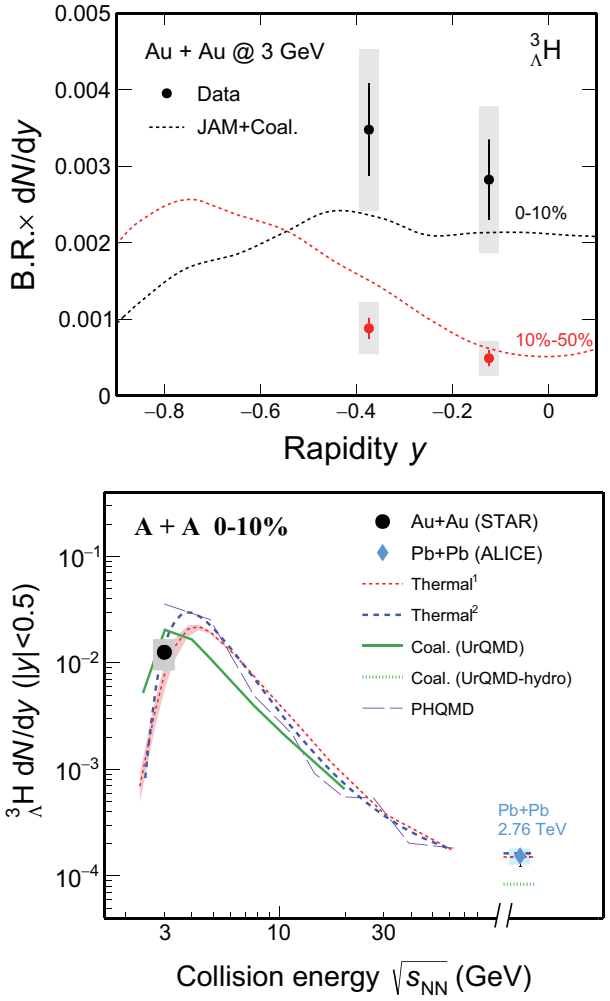

Fig. 8. (Color online) Top panel is the B.R.× dN/dy as a function of rapidity for $^3_\Lambda$H yield in 0–10% and 10%–50% centrality Au + Au collisions at $\sqrt{s_{NN}}$ = 3 GeV [27]. Bottom panel is the $^3_\Lambda$H yield at mid-rapidity as a function of $\sqrt{s_{NN}}$ in central heavy-ion collisions [27,30]. Symbols represent measurements and lines are theoretical calculations. Thermal[1] is the calculation from Ref. [54] and Thermal[2] comes from Ref. [43]. Data points at bottom panel assume a B.R. of 25% for the two-body pionic decay channel from theoretical calculation [55].

portation Model (JAM) [46] is used to model the dynamical stage of the reaction [27]. The coalescence prescription, which is well formulated in studying the cluster formation in heavy-ion collisions [47–52], is subsequently applied to the produced hadron as an afterburner [27]. In this calculation [46,53], deuterons are formed through the coalescence of proton and neutron, and subsequently, $^3_\Lambda$H is formed through the coalescence of Λ with deuteron. The coalescence takes place if the relative momentum of the deuteron and Λ is within a sphere of radius p_C and the spacial coordinates is within a sphere of radius of r_C. It is found that calculations with coalescence parameters (p_C, r_C) of (0.12 GeV/c, 4 fm) reproduce the centrality and rapidity dependence of the $^3_\Lambda$H yield in Au + Au collisions at $\sqrt{s_{NN}} = 3$ GeV reasonable well, shown as the dashed curves in Fig. 8. This implies that the coalescence mechanism is able to explain the measured data. Together with the $^4_\Lambda$H yield measurement in Ref. [27], the data offer quantitative input on the coalescence parameters for hypernuclei formation in the high baryon density region, enabling more accurate estimations of the production yields of exotic strange objects [43].

The study of mid-rapidity yields for central collisions over a broad collision energy will shed more light on the light hypernuclei production mechanism in heavy-ion collisions because the energy

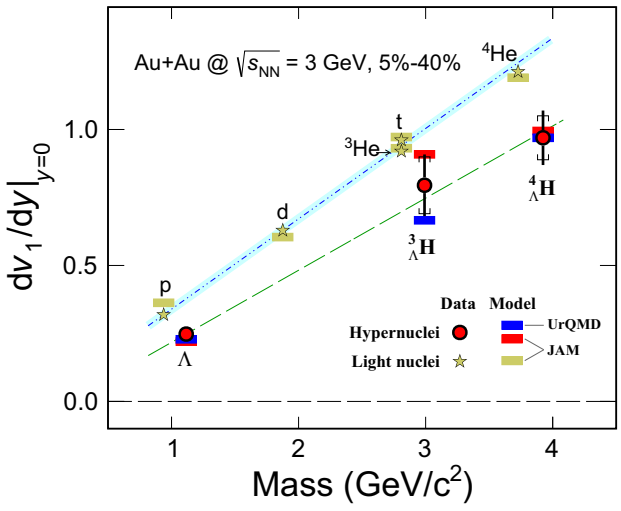

Fig. 9. (Color online) Mass dependence of the mid-rapidity v_1 slope, the dv_1/dy for Λ, $^3_\Lambda$H and $^4_\Lambda$H from mid-central Au + Au collisions at $\sqrt{s_{NN}} = 3$ GeV [68]. Symbols represent measurements, while boxes represent transport model calculations.

density, or more related the effective degree of freedom of the system created in $\sqrt{s_{NN}} = 3$ GeV [56] is distinguished different from those created at TeV energy [57]. In addition to the aforementioned coalescence model, thermal model is another approach extensively adopted to describe the nucleosynthesis in heavy-ion collisions [54]. Current thermal models do not make any assumption on the structure of the hypernucleus and treat it as a point like particle [54]. However, the dependence of the production on the system configuration is very similar to the coalescence model [50]. Bottom panel of Fig. 8 shows the total dN/dy as a function of center-of-mass energy from a few GeV to a few TeV, with a B.R. of 25% from theoretical calculation for the $^3_\Lambda\mathrm{H} \to {}^3\mathrm{He} + \pi^-$ [55]. By comparing the yields with the theoretical calculations, one sees that canonical ensemble thermal model [54] can approximately describe the $^3_\Lambda$H data over a few orders of magnitude of $\sqrt{s_{NN}}$. It is noted that canonical ensemble thermal statistics is mandatory to account for the large ϕ/K^- and ϕ/Ξ^- ratios measured at low energy [58]. Coalescence calculation by the Ultra-Relativistic Quantum Molecular Dynamics Model (UrQMD) [59] is consistent with the $^3_\Lambda$H yield at Au + Au collisions of $\sqrt{s_{NN}} = 3$ GeV, whereas the UrQMD-hydro hybrid model underestimates the yield at Pb + Pb collisions of $\sqrt{s_{NN}} = 2.76$ TeV [60,61]. This may reflect the fact that baryon-antibaryon annihilation is largely different from collisions of a few GeV to a few TeV, due to the longer evolution time in the hadronic stage at higher collision energies. Production yield of $^3_\Lambda$H also depends on its structure in the coalescence calculation, including the processes $\mathrm{p} + \mathrm{n} + \Lambda \to {}^3_\Lambda\mathrm{H}$ and $\mathrm{d} + \Lambda \to {}^3_\Lambda\mathrm{H}$, the yield of $^3_\Lambda$H is found to be enhanced by about a factor of two compared to the calculation only considering process $\mathrm{p} + \mathrm{n} + \Lambda \to {}^3_\Lambda\mathrm{H}$ [62]. Calculations from Parton-Hadron-Quantum-Molecular-Dynamics (PHQMD) [63,64], which utilizes a dynamical description of hypernuclei formation approach, is consistent with the measured yield within uncertainties. It is noted that measurement of the production yield of $^3_\Lambda$H in p + Pb collision at $\sqrt{s_{NN}}$ = 5.02 GeV has been reported recently [45]. The measured dN/dy leads to the exclusion with a significance larger than 6σ of some configurations of the thermal statistical model [45]. The measured $^3_\Lambda\mathrm{H}/\Lambda$ ratio is well described by the two-body coalescence prediction [65] while disfavoured the three-body formulation [45,65]. It is stated in the summary of Ref. [45] that it remains to be seen if advanced version of thermal statistical model using the S-matrix approach account for the interactions among hadrons [66] will be able to describe the data.

Looking at both panels of Fig. 8, it is worth mentioning that baryonic interactions in PHQMD are modeled by density dependent two-body baryonic potentials while JAM model adopts a baryonic mean-field approach. Since ${}^{3}_{\Lambda}$H is a fragile object, it is mostly likely formed at later time of the collisions where the density is low enough that the objects formed are not immediately destroyed. Thus, experimental and theoretical studies on the production yields not only provide quantitative input on the production mechanisms of loosely bound objects in heavy-ion collisions, but may also give information on the time evolution of the high baryon density medium formed [67].

Another interesting observable is the excitation function of hypernuclei collective flow, which may provide valuable information for understanding the in-medium Y-N interaction [68–71]. It will also provide the possibility to build a connection between heavy-ion collision and the equation-of-state of high baryon density matter which governs the inner structure of compact stars [72]. Collective flow is driven by the pressure gradient created in such collisions, which has been commonly used for studying the properties of nuclear matter created in collisions [73–75]. Experimentally, it is convenient to quantify flow by the Fourier coefficient of the particle distribution in emission azimuthal angle, measured with respect to the reaction plane. We focus on the first harmonic of the distribution, the so-called directed flow (v_1). The word "directed" comes from the fact that such flow looks like a sideward bounce of the fragments away from each in the reaction plane.

Fig. 9 shows the slope of the $\mathrm{d}v_1/\mathrm{d}y$ near mid-rapidity for ${}^{3}_{\Lambda}$H, together with Λ and ${}^{4}_{\Lambda}$H as a function of particle mass in 5%–40% Au + Au collisions at $\sqrt{s_{\mathrm{NN}}}$ = 3 GeV [68]. Measurements on p, d, t, ^{3}He and ^{4}He in the similar kinematic window to Λ and light hypernuclei have also been performed and plotted for comparison [68]. The slopes $\mathrm{d}v_1/\mathrm{d}y$ of hypernuclei are systematically lower than those of light nuclei with the same mass number. Linear fits are performed on the mass dependence of $\mathrm{d}v_1/\mathrm{d}y$ for both light nuclei and hypernuclei. The slope parameters are 0.3323 ± 0.0003 for light nuclei and 0.27 ± 0.04 for hypernuclei, respectively. Within uncertainties, it seems that the mass dependence of the slope of hypernuclei v_1 is similar, but not compatible to that of light nuclei. Calculations from transport models (JAM and UrQMD) plus coalescence as afterburner are in agreement with data within uncertainties [68]. These observations suggest that coalescence of nucleons and Λ could be the dominant mechanism for the ${}^{3}_{\Lambda}$H production in Au + Au collisions at $\sqrt{s_{\mathrm{NN}}}$ = 3 GeV. The measurement may open up a new direction for studying Y-N interaction under finite pressure [71].

Recently, new results on precision measurements of Λ-p elastic scattering from Jefferson Lab [76] and Σ^{-}-p elastic scattering from Japan Proton Accelerator Research Complex (J-PARC) [77] became available, which may help to constrain the equation-of-state of high density matter inside a neutron star. Systematic studies of momentum correlation functions between proton and hyperons in pp or AA collisions at RHIC or LHC energies provide valuable information to constrain the Y-N interactions [78,79]. Such as the measurement on the interaction of pΛ pairs from zero relative momentum up to the opening of NΣ channel yields to a weaker N$\Sigma\rightarrow$NΛ coupling would require a more repulsive three-body NNΛ interaction for a proper description of the hyperon in-medium properties, which has implications on the nuclear equation-of-state and for the presence of hyperons inside neutron stars [78]. Similar study has been preformed in electron–positron collisions. The $\Xi^0 n \rightarrow \Xi^- p$ is observed by using huge J/Ψ events collected with the Beijing Spectrometer Experiment detector operating at the Beijing Electron Positron Collider storage ring [80]. This is the first study of Y-N interaction in electron–positron collisions, and opens up a new direction for such research [81].

4. Discussion

There have been several discussions around the $\tau({}^{3}_{\Lambda}\mathrm{H})$ measurements since the 1960s [19,82]. The topic is of considerable interest especially in view of the short values, such as the $\tau({}^{3}_{\Lambda}\mathrm{H}) = (90^{+220}_{-40})$ ps from Ref. [19] in comparison with the $\tau_\Lambda = (263.2 \pm 2.0)$ ps [18]. It is learnt that lifetime measurements using visual detectors are notoriously difficult because hypernuclei are in general produced with low kinetic energies and the majority are brought to rest before decay. Determinations of the lifetimes depend on samples in which only very few decay in flight are challenging. Nevertheless, there are nuclear emulsion measurements for the lifetime of light hypernuclei including ${}^{3}_{\Lambda}$H and a helium bubble chamber measurement for ${}^{3}_{\Lambda}$H. From the results shown in Fig. 4, one sees that some early measurements [19,22] indicate that ${}^{3}_{\Lambda}$H has a shorter lifetime than the free Λ. In particular, the lifetime measurement from Ref. [22] was $\tau({}^{3}_{\Lambda}\mathrm{H}) = (128^{+35}_{-26})$ ps, which presented the smallest error among similar studies in the 1960s and 70s, and was shorter than the others. This measurement was based on the three-body decay channel ${}^{3}_{\Lambda}\mathrm{H} \rightarrow \mathrm{p} + \mathrm{d} + \pi^-$ in a nuclear emulsion experiment. The shorter lifetime was attributed to the dissociation of the lightly-bound Λ and deuteron when they are traveling in a dense medium [83]. However, this explanation is not very satisfying, since measurements performed in Refs. [20,21,24] also used nuclear emulsion, yet their measurements were close to the τ_Λ. In addition, Ref. [19] used a helium bubble chamber that should not be affected by the hypothesized dissociation, had the lifetime values lower than the free Λ. Thus, Prof. Davis [25] and Prof. Dalitz [26] commented that the issue was not addressed yet. Recent heavy-ion experiments have been carried out to address this issue. Measurements of $\tau({}^{3}_{\Lambda}\mathrm{H})$ from experiments at the RHIC-STAR, at the Heavy-Ion-Synchrotron Hypernuclear spectroscopy (SIS18-HypHI), and at the LHC-ALICE were reported [15,27–32]. These data showed the $\tau({}^{3}_{\Lambda}\mathrm{H})$ value $\approx (0.5 - 0.96)\tau_\Lambda$, presenting a similar large spread of the $\tau({}^{3}_{\Lambda}\mathrm{H})$ values, as observed in the older nuclear emulsion and helium bubble chamber measurements (c.f. Fig. 4).

On the other hand, there has been much interest in applying effective field theory (EFT) methods to nuclear systems with two or more nucleons. EFTs provide a powerful framework to explore a separation of scales in physical systems in order to perform systematic, model-independent calculations [84]. Calculation of important quantities in nuclear physics using lattice QCD is becoming practical, usually at the physical values of strange quark but not at the physical value of light-quark masses [85]. Closely related to the topic of current paper, calculations [55] based on a ${}^{3}_{\Lambda}$H wave function and 3 N scattering states from rigorous solution of three-body Faddeev equations using realistic N-N and Y-N interactions yielded a lifetime only 3% smaller than the τ_Λ. It is worth mentioning that the τ_Λ from Ref. [55] is 272 ps, which is 3% larger than the world data [18]. A simple model calculations [16] by taking the Λ to orbit an unperturbed deuteron in a Λ-deuteron potential based on a separable Λ-nucleon potential predicted a lifetime $\approx$13% smaller than the τ_Λ. In such study, the author found that as long as the Λ separation energy of ${}^{3}_{\Lambda}$H is reproduced, the lifetime calculation is rather insensitive to the fine details of the particular ΛN interaction model chosen [16]. Within a closure-approximation calculation in which the associated exchange matrix element is evaluated with wave functions obtained by solving the ${}^{3}_{\Lambda}$H three-body Faddeev equation, Ref. [86] had the result $\tau({}^{3}_{\Lambda}\mathrm{H}) \approx 0.90\tau_\Lambda$. Introducing π final state interaction in terms of π distorted scattering waves in Ref. [86] results in $\tau({}^{3}_{\Lambda}\mathrm{H}) \approx 0.81\tau_\Lambda$. Different calculations seem to cover the measurements worldwide. A much more precise measurement will be important to pin down the potential different physics involved in different calculations.

Since the ${}^{3}_{\Lambda}$H lifetime and Λ separation energy are strongly correlated, we can explore the underlying physics by the Λ separation energy measurements. π exchange studies using a closure approximation to sum over the final nuclear states reached in the ${}^{3}_{\Lambda}$H weak decay, reduced the ${}^{3}_{\Lambda}$H lifetime calculation to the evaluation of a ${}^{3}_{\Lambda}$H matrix element [82,87]. With a choice of the closure energy $q = 96$ MeV/c, Rayet and Dalitz deduced the correlation between lifetime and binding as $\Gamma({}^{3}_{\Lambda}\mathrm{H}, J = \frac{1}{2}) = (1 + 0.14\sqrt{B_\Lambda})\Gamma_\Lambda$ [82]. Calculation based on pionless effective field theory (∌EFT) with Λ and deuteron degrees of freedom shows that the sensitivity of the total width to binding energy is small, while the partial widths for decays into individual final states and the ratio $R = \Gamma_{^3\mathrm{He}}/(\Gamma_{^3\mathrm{He}} + \Gamma_{pd})$ is large [17,88]. That is, the R value will increase quite significantly as B_Λ increased. It seems that the R quantity appears to be better suited to determine B_Λ indirectly than the total width [16,24]. Employing ${}^{3}_{\Lambda}$H and ^{3}He three-body wave functions generated by *ab initio* hypernuclear no-core shell model, microscopic calculation [89] of the ${}^{3}_{\Lambda}$H mesonic decay rate $\Gamma({}^{3}_{\Lambda}\mathrm{H} \to {}^{3}\mathrm{He} + \pi^-)$ found that: (i) replacing pionic plane wave by realistic $\pi^- - {}^{3}$He distorted wave enhances the decay rate by ≈15%. (ii) The ΣNN admixtures in ${}^{3}_{\Lambda}$H reduce the purely ΛNN decay rate by ≈10% due to interference effects. Their calculation also suggests that the $\tau({}^{3}_{\Lambda}\mathrm{H})$ varies strongly with the rather poorly known Λ separation energy. One learns that such poorly known B_Λ serves as a free-parameter entering into the EFT and can be varied without changing other observables [17,88]. The B_Λ is one of the key quantities to discriminate different theoretical scenarios [90].

Fig. 10 shows the correlation of $\tau({}^{3}_{\Lambda}\mathrm{H})$ and B_Λ of the ${}^{3}_{\Lambda}$H. The pink curve represents the χEFT calculation with different harmonic oscillator basis ultraviolet scales [89]. The color black curve is from π exchange calculation [82] while the color blue is the result from ∌EFT [88]. Bands represent uncertainties of each calculations. The χEFT is able to associate different measurements of $\tau({}^{3}_{\Lambda}\mathrm{H})$ with its own underlying values of B_Λ [89,91]. We here plot the world average values from Figs. 4 and 6 instead of putting each individual measurement. We see on Fig. 10 that the average value is consistent with calculations from π exchange theory, ∌EFT, χEFT considering the data uncertainties and the calculation uncertainties.

There had been discussions on the partial mesonic decay rate to the total rate mainly because the branching ratio for various decay modes of a hypernucleus will generally depend on both the spin of the hypernucleus and the nature of the Λ decay interaction [92,93].

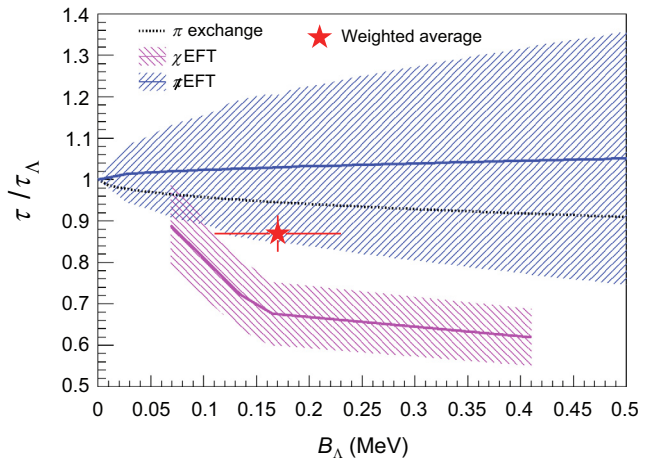

Fig. 10. (Color online) Correlation of the ${}^{3}_{\Lambda}$H lifetime relative to the free Λ lifetime as a function of the Λ separation of ${}^{3}_{\Lambda}$H. Data point is the average of world data, and curves are calculations from π exchange [82], pionless effective field theory [88] and chiral effective field theory [89].

From experimental side, it is challenging to measure the absolute decay rate but more straight forward to measure the ratio of different decay modes by conducting different decay modes in the same experiment. For the ${}^{3}_{\Lambda}$H, this ratio is defined as $R_3 = \frac{\Gamma({}^{3}_{\Lambda}\mathrm{H} \to {}^{3}\mathrm{He} + \pi^-)}{\Gamma({}^{3}_{\Lambda}\mathrm{H} \to \text{all } \pi^- \text{ channels})}$. It had been measured by different experiment from early days [20,24,94] and the modern heavy-ion collisions [31], with all data being consistent with the average value of $R_3 = 0.35 \pm 0.04$, and being consistent under the assumption $J({}^{3}_{\Lambda}\mathrm{H}) = \frac{1}{2}$ within data uncertainties. On-going measurement with uncertainty less than 10% is progressing well and may provide stringent constrains in model calculation [95].

5. Summary

We discuss measurements of lifetime, Λ separation energy, production yields and collective flow on the lightest known hypernuclei, the ${}^{3}_{\Lambda}$H to gain knowledge of the Y-N interaction. Both lifetime and Λ separation energy data show a large spread among different measurements, thus we perform a statistical analysis to include all data. The average values are $\tau({}^{3}_{\Lambda}\mathrm{H}) = (228.5 \pm 11.6)$ ps, $B_\Lambda = (0.17 \pm 0.06)$ MeV, while the $\tau({}^{3}_{\Lambda}\mathrm{H}) = (236.4 \pm 8.1)$ ps is an average analysis of measurements in heavy-ion collisions. Those values serve as input parameters to constrain the effective field theory calculations. Considering the large uncertainties in the measurements and theoretical calculations, different scenarios of calculations can describe the average values. Data on production yields and directed flow are well described by the transport model plus coalescence afterburner calculations, in which interactions among nucleons and strange baryons are important ingredients. Data on ${}^{3}_{\Lambda}\bar{\mathrm{H}}$ to ${}^{3}_{\Lambda}$H mass difference is consistent with zero within 10^{-4} precision. Independent and on-going measurements with better precision will be helpful to nail down the possible systematic and shed light on the structure of the ${}^{3}_{\Lambda}$H and the Y-N interaction. Further theoretical development for hypernucleus is also expected.

6. Perspective

In the last two decades, the relativistic heavy-ion collisions have proved to be an effective way of producing the simplest hypernucleus and studying its properties since such measurement [96] at Alternating Gradient Synchrotron (AGS) was first performed in the early 2000s several decades after the last experimental emulsion measurements of ${}^{3}_{\Lambda}$H in the 1970s. In the last decade, the improved detector capabilities and increased statistics at RHIC and the LHC facilities have offered unique opportunities for precise measurements of lifetime and Λ separation energy. The precision of lifetime measurement has significantly improved to be ±10 ps while the Λ separation energy measurement has been hovering around 50 – 100 keV with an improved control and understanding of the systematical uncertainties. To date, the world-average lifetime measurement shows a 3σ significance lower than the free Λ lifetime with a precision of ±10 ps. With the improved detector capability and increased high-statistical data of ALICE Detector at the LHC [15] and STAR Detector at RHIC [27], this would be further improved in the near future. A1 at Mainz Microtron [97] using novel high-luminosity lithium target and E07 at J-PARC [98] using machine learning on analyzing emulsion data are promising in producing the most precise measurements of the Λ separation energy with a precision of ±20 – 30 keV in the near future. New measurement of hypernucleus lifetime using in-flight ${}^{4}\mathrm{He}(K^-, \pi^0){}^{4}_{\Lambda}\mathrm{H}$ reaction has obtained $\tau({}^{4}_{\Lambda}\mathrm{H}) = (206 \pm 8(\text{stat.}) \pm 12(\text{syst.}))$ ps, one of the most precise measurements to date [99]. They are preparing to measure the lifetime of ${}^{3}_{\Lambda}$H using the same setup in the near

future [100]. These should provide measurements of a non-zero value with more than 5σ significance if the nominal values of the world-average Λ separation energy and lifetime (different from Λ) hold. The endeavor in the recent decades would finally provide solid experimental input for further theory developments.

Conflict of interest

The authors declare that they have no conflict of interest.

Acknowledgments

We thank S. Wang for helping design Fig. 1. J. Chen was supported in part by the National Key Research and Development Program of China (2022YFA1604900) and the National Natural Science Foundation of China (NSFC) (12025501). Y.-G. Ma was supposed in part by the NSFC (11890710, 11890714, and 12147101). X. Dong and Z. Xu were funded by the U.S. DOE Office of Science (DE-sc0012704, DE-FG02-10ER41666, DE-AC02-98CH10886, and DE-KB0201022).

Author contributions

Jinhui Chen, Xin Dong, Yu-Gang Ma, and Zhangbu Xu worked together on the preparation, discussion and write-up of the paper. They contributed equally to this work.

References

[1] Gross DJ, Wilczek F. Ultraviolet behavior of nonabelian gauge theories. Phys Rev Lett 1973;30:1343–6.
[2] Politzer HD. Reliable perturbative results for strong interactions? Phys Rev Lett 1973;30:1346–9.
[3] Aprahamian A, Atcher R, Helen C, et al. Reaching for the horizon: the 2015 long range plan for nuclear science 2015; https://www.osti.gov/biblio/1296778.
[4] Itoh N. Hydrostatic equilibrium of hypothetical quark stars. Prog Theor Phys 1970;44:291.
[5] Danysz M, Pniewski J. Delayed disintegration of a heavy nuclear fragment: I. Phil Mag 1953;44:348–50.
[6] Lattimer JM, Prakash M. The physics of neutron stars. Science 2004;304:536–42.
[7] Tolos L, Fabbietti L. Strangeness in nuclei and neutron stars. Prog Part Nucl Phys 2020;112:103770 .
[8] Chrien RE, Dover CB. Nuclear systems with strangeness. Ann Rev Nucl Part Sci 1989;39:113–50.
[9] Hashimoto O, Tamura H. Spectroscopy of Lambda hypernuclei. Prog Part Nucl Phys 2006;57:564–653.
[10] Shuryak EV. Quantum chromodynamics and the theory of superdense matter. Phys Rept 1980;61:71–158.
[11] Chen JH, Keane D, Ma YG, et al. Antinuclei in heavy-ion collisions. Phys Rept 2018;760:1–39.
[12] Gal A, Hungerford EV, Millener DJ. Strangeness in nuclear physics. Rev Mod Phys 2016;88:035004.
[13] Juric M, Bohm G, Klabuhn J, et al. A new determination of the binding-energy values of the light hypernuclei ($A \leq 15$). Nucl Phys B 1973;52:1–30.
[14] STAR Collaboration, Adam J, et al. Measurement of the mass difference and the binding energy of the hypertriton and antihypertriton. Nat Phys 2020;16:409–412.
[15] ALICE Collaboration, Acharya S, et al. Measurement of the lifetime and Λ separation energy of $^{3}_{\Lambda}$H. Phys Rev Lett 2023;131:102302.
[16] Congleton JG. A simple model of the hyper triton. J Phys G 1992;18:339.
[17] Hildenbrand F, Hammer HW. Three-body hypernuclei in pionless effective field theory. Phys Rev C 2019;100:034002 [Erratum. Phys Rev C 2020;102:039901].
[18] Particle Data Group, Workman RL, et al. Review of particle physics. Prog Theor Exp Phys 2022;2022:083C01.
[19] Prem RJ, Steinberg PH. Lifetime of hypernuclei, $^{3}_{\Lambda}$H, $^{4}_{\Lambda}$H, $^{5}_{\Lambda}$H. Phys Rev 1964;136:B1803.
[20] Keyes G, Derrick M, Fields T, et al. New measurements of the $^{3}_{\Lambda}$H lifetime. Phys Rev Lett 1968;20:819.
[21] Phillips RE, Schneps J. Lifetime of light hyperfragments. Phys Rev 1969;180:1307.
[22] Bohm G, Klabuhn J, Krecker U, et al. On the lifetime of the $^{3}_{\Lambda}$H hypernucleus. Nucl Phys B 1970;16:46.
[23] Keyes G, Derrick M, Fields T, et al. Properties of $^{3}_{\Lambda}$H. Phys Rev D 1970;1:66.
[24] Keyes G, Sacton J, Wickens JH, et al. A measurement of the lifeimt of the $^{3}_{\Lambda}$H hypernucleus. Nucl Phys B 1973;67:269.
[25] Davis DH. 50 years of hypernuclear physics. I. The early experiments. Nucl Phys A 2005;754:3–13.
[26] Dalitz RH. 50 years of hypernuclear physics. 2. The later years. Nucl Phys A 2005;754:14–24.
[27] ASTAR Collaboration, Abdallah M, et al. Measurements of $^{3}_{\Lambda}$H and $^{4}_{\Lambda}$H lifetimes and yields in Au+Au collisions in the high baryon density region. Phys Rev Lett 2022;128:202301.
[28] STAR Collabration, Abelev BI, et al. Observation of an antimatter hypernucleus. Science 2010;328:58–62.
[29] Rappold C, Kim E, Nakajima D, et al. Hypernuclear spectroscopy of products from ^{6}Li projectiles on a carbon target at 2 *A* GeV. Nucl Phys A 2013;913:170–84.
[30] ALICE Collaboration, Adam J, et al. $^{3}_{\Lambda}$H and $^{3}_{\Lambda}\bar{\mathrm{H}}$ production in Pb-Pb collisions at $\sqrt{s_{\mathrm{NN}}} = 2.76$ TeV. Phys Lett B 2016;754:360–372.
[31] STAR Collaboration, Adamczyk L, et al. Measurement of the $^{3}_{\Lambda}$H lifetime in Au+Au collisions at the BNL Relativistic Heavy Ion Collider. Phys Rev C 2018;97:054909.
[32] ALICE Collaboration, Acharya S, et al. $^{3}_{\Lambda}$H and $^{3}_{\Lambda}\bar{\mathrm{H}}$ lifetime measurement in Pb-Pb collisions at $\sqrt{s_{\mathrm{NN}}} = 5.02$ TeV via two-body decay. Phys Lett B 2019;797:134905.
[33] Gajewski W, Mayeur C, Sacton J, et al. A compilation of binding energy values of light hypernuclei. Nucl Phys B 1967;1:105–13.
[34] Bohm G, Klabuhn J, Krecker U, et al. A determination of the binding-energy values of light hypernuclei. Nucl Phys B 1968;4:511–26.
[35] Liu P, Chen J, Keane D, et al. Recalibration of the binding energy of hypernuclei measured in emulsion experiments and its implications. Chin Phys C 2019;43:124001.
[36] Gogami T, Chen C, Kawama D, et al. High resolution spectroscopic study of $^{10}_{\Lambda}$Be. Phys Rev C 2016;93: 034314.
[37] Botta E, Bressani T, Feliciello A. On the binding energy and the charge symmetry breaking in A $\leqslant$ 16 Λ-hypernuclei. Nucl Phys A 2017;960:165–79.
[38] Adam J, Adamova D, Aggarwal MM, et al. Precision measurement of the mass difference between light nuclei and anti-nuclei with the ALICE experiment at the LHC. Nat Phys 2015;11:811–814.
[39] Agakishiev H, Aggarwal M, Ahammed Z, et al. Observation of the antimatter helium-4 nucleus. Nature 2011;473:353 [Erratum: Nature 2011;475:412].
[40] ALICE Collaboration, Acharya S, et al. Production of ^{4}He and $^{4}\overline{\mathrm{He}}$ in Pb-Pb collisions at $\sqrt{s_{\mathrm{NN}}}$ = 2.76 TeV at the LHC. Nucl Phys A 2018;971:1–20.
[41] Gabrielse G, Khabbaz A, Hall DS, et al. Precision mass spectroscopy of the anti-proton and proton using simultaneously trapped particles. Phys Rev Lett 1999;82:3198–201.
[42] Armstrong TA, Barish K, Batsouli S, et al. Mass dependence of light nucleus production in ultrarelativistic heavy ion collisions. Phys Rev Lett 1999;83:5431–4.
[43] Steinheimer J, Gudima K, Botvina A, et al. Hypernuclei, dibaryon and antinuclei production in high energy heavy ion collisions: thermal production versus coalescence. Phys Lett B 2012;714:85–91.
[44] Zhang L, Zhang S, Ma YG. Production of ωnn and $\omega\omega n$ in ultra-relativistic heavy-ion collisions. Eur Phys J C 2022;82:416.
[45] ALICE Collaboration, Acharya S, et al. Hypertriton production in p-Pb collisions at $\sqrt{s_{\mathrm{NN}}}$=5.02 TeV. Phys Rev Lett 2022a;128:252003.
[46] Nara Y, Otuka N, Ohnishi A, et al. Study of relativistic nuclear collisions at AGS energies from p + Be to Au + Au with hadronic cascade model. Phys Rev C 2000;61: 024901.
[47] Cho S, Furumoto T, Hyodo T, et al. Studying exotic hadrons in heavy-ion collisions. Phys Rev C 2011;84:064910.
[48] Liu P, Chen JH, Ma YG, et al. Production of light nuclei and hypernuclei at High Intensity Accelerator Facility energy region. Nucl Sci Tech 2017;28:55 [Erratum: Nucl Sci Tech 2017;28:89].
[49] Shao T, Chen J, Ko CM, et al. Yield ratio of hypertriton to light nuclei in heavy-ion collisions from $\sqrt{s_{\mathrm{NN}}}$ = 4.9 GeV to 2.76 TeV. Chin Phys C 2020;44:114001.
[50] Hillmann P, Käfer K, Steinheimer J, et al. Coalescence, the thermal model and multi-fragmentation: the energy and volume dependence of light nuclei production in heavy ion collisions. J Phys G 2022;49:055107.
[51] Zhang L, Chen J, Li W, et al. Implication of two-baryon azimuthal correlations in pp collisions at LHC energies on the QGP. Phys Lett B 2022;829:137063 .
[52] Zhu LL, Wang B, Wang M, et al. Energy and centrality dependence of light nuclei production in relativistic heavy-ion collisions. Nucl Sci Tech 2022;33:45.
[53] Liu H, Zhang D, He S, et al. Light nuclei production in Au+Au collisions at $\sqrt{s_{\mathrm{NN}}}$ = 5–200 GeV from JAM model. Phys Lett B 2020;805:135452 [Erratum: Phys Lett B 2022;829:137132].
[54] Andronic A, Braun-Munzinger P, Stachel J, et al. Production of light nuclei, hypernuclei and their antiparticles in relativistic nuclear collisions. Phys Lett B 2011;697:203–7.
[55] Kamada H, Golak J, Miyagawa K, et al. Pi mesonic decay of the hypertriton. Phys Rev C 1998;57:1595–603.
[56] STAR Collaboration, Abdallah MS, et al. Disappearance of partonic collectivity in $\sqrt{s_{\mathrm{NN}}}$= 3 GeV Au+Au collisions at RHIC. Phys Lett B 2022;827:137003.
[57] Muller B, Schukraft J, Wyslouch B. First Results from Pb+Pb collisions at the LHC. Ann Rev Nucl Part Sci 2012;62:361–86.
[58] STAR Collaboration, Abdallah MS, et al. Probing strangeness canonical ensemble with K^-, $\phi(1020)$ and Ξ^- production in Au+Au collisions at $\sqrt{s_{\mathrm{NN}}}$ = 3 GeV. Phys Lett B 2022;831:137152.

[59] Bleicher M, Zabrodin E, Spieles C, et al. Relativistic hadron hadron collisions in the ultrarelativistic quantum molecular dynamics model. J Phys G 1999;25:1859–96.
[60] Petersen H, Steinheimer J, Burau G, et al. A fully integrated transport approach to heavy ion reactions with an intermediate hydrodynamic stage. Phys Rev C 2008;78:044901.
[61] Zhao W, Zhu L, Zheng H, et al. Spectra and flow of light nuclei in relativistic heavy ion collisions at energies available at the BNL Relativistic Heavy Ion Collider and at the CERN Large Hadron Collider. Phys Rev C 2018;98:054905.
[62] Zhang Z, Ko CM. Hypertriton production in relativistic heavy-ion collisions. Phys Lett B 2018;780:191–5.
[63] Aichelin J, Bratkovskaya E, Le Fèvre A, et al. Parton-hadron-quantum-molecular dynamics: a novel microscopic *n*-body transport approach for heavy-ion collisions, dynamical cluster formation, and hypernuclei production. Phys Rev C 2020;101:044905 .
[64] Gläßel S, Kireyeu V, Voronyuk V, et al. Cluster and hypercluster production in relativistic heavy-ion collisions within the parton-hadron-quantum-molecular-dynamics approach. Phys Rev C 2022;105:014908.
[65] Sun KJ, Ko CM, Dönigus B. Suppression of light nuclei production in collisions of small systems at the Large Hadron Collider. Phys Lett B 2019;792:132–7.
[66] Cleymans J, Lo PM, Redlich K, et al. Multiplicity dependence of (multi)strange baryons in the canonical ensemble with phase shift corrections. Phys Rev C 2021;103:014904.
[67] Braun-Munzinger P, Dönigus B. Loosely-bound objects produced in nuclear collisions at the LHC. Nucl Phys A 2019;987:144–201.
[68] STAR Collaboration, Aboona B, et al. Observation of directed flow of hypernuclei $^{3}_{\Lambda}$H and $^{4}_{\Lambda}$H in $\sqrt{s_{NN}}$ = 3 GeV Au+Au collisions at RHIC. Phys Rev Lett 2023;130:212301.
[69] Nara Y, Niemi H, Ohnishi A, et al. Examination of directed flow as a signature of the softest point of the equation of state in QCD matter. Phys Rev C 2016;94:034906.
[70] Nara Y, Niemi H, Steinheimer J, et al. Equation of state dependence of directed flow in a microscopic transport model. Phys Lett B 2017;769:543–8.
[71] Ma YG. Hypernuclei as a laboratory to test hyperon-nucleon interactions. Nucl Sci Tech 2023;34:97.
[72] Stoecker H. Collective flow signals the quark gluon plasma. Nucl Phys A 2005;750:121–47.
[73] Ollitrault JY. Anisotropy as a signature of transverse collective flow. Phys Rev D 1992;46:229–45.
[74] Ma YG. The colective flow from the degree of freedom of nucleons to quarks. J Fudan University (Natural Sci) 2023;62:73.
[75] Wang H, Chen JH. Anisotropy flows in Pb–Pb collisions at LHC energies from parton scatterings with heavy quark trigger. Nucl Sci Tech 2022;33:15.
[76] CLAS Collaboration, Rowley J, et al. Improved Λp elastic scattering cross sections between 0.9 and 2.0 GeV/c and connections to the neutron star equation of state. Phys Rev Lett 2021;127:272303.
[77] J-PARC E40 Collaboration, Miwa K, et al. Precise measurement of differential cross sections of the $\Sigma^- p \to \Lambda n$ reaction in momentum range 470–650 MeV/c. Phys Rev Lett 2022;128:072501.
[78] Acharya S, Adamova D, Adler A, et al. Exploring the NΛ–NΣ coupled system with high precision correlation techniques at the LHC. Phys Lett B 2022; 833:137272.
[79] STAR Collaboration, Adam J, et al. The proton-Ω correlation function in Au+Au collisions at $\sqrt{s_{NN}}$=200 GeV. Phys Lett B 2019;790:490–7.
[80] BESIII Collaboration, Ablikim M, et al. First study of reaction $\Xi^0 n \to \Xi^- p$ using Ξ^0-nucleus scattering at an electron-positron collider. Phys Rev Lett 2023;130:251902.
[81] Yuan CZ, Karliner M. Cornucopia of antineutrons and hyperons from a super J/ψ factory for next-generation nuclear and particle physics high-precision experiments. Phys Rev Lett 2021;127:012003.
[82] Rayet M, Dalitz RH. The lifetime of $^{3}_{\Lambda}$H. Nuovo CIMENTO A 1966;46:786.
[83] Bohm G, Wysotzki F. Coulomb disintegration of $^{3}_{\Lambda}$H in nuclear emulsion. Nucl Phys B 1970;15:628–36.
[84] Weinberg S. Nuclear forces from chiral Lagrangians. Phys Lett B 1990;251:288–92.
[85] Beane SR, Chang E, Cohen SD, et al. Light nuclei and hypernuclei from Quantum Chromodynamics in the limit of SU(3) flavor symmetry. Phys Rev D 2013;87:034506.
[86] Gal A, Garcilazo H. Towards resolving the $^{3}_{\Lambda}$H lifetime puzzle. Phys Lett B 2019;791:48–53.
[87] Dalitz RH, Rajasekharan G. The spins and lifetimes of the light hypernuclei. Phys Lett 1962;1:58–60.
[88] Hildenbrand F, Hammer HW. Lifetime of the hypertriton. Phys Rev C 2020;102:064002 .
[89] Pérez-Obiol A, Gazda D, Friedman E, et al. Revisiting the hypertriton lifetime puzzle. Phys Lett B 2020;811:135916 .
[90] Le H, Haidenbauer J, Meißner UG, et al. Implications of an increased Λ-separation energy of the hypertriton. Phys Lett B 2020;801:135189 .
[91] Gazda D, Pérez-Obiol A, Gal A, et al. Hypertriton lifetime 2023. arXiv: 2310.03087, 2023.
[92] Leon M. Decay of $^{3}_{\Lambda}$H and the spin dependence of the lambda-nucleon interaction. Phys Rev 1959;113:1604–7.
[93] Dalitz RH, Liu L. Pionic decay modes of light lambda hypernuclei. Phys Rev 1959;116:1312–21.
[94] Bertrand D, Coremans G, Mayeur C, et al. Branching ratios for the pi-mesonic decays of the hypernuclei $^{3}_{\Lambda}$H and $^{3}_{\Lambda}$H. Nucl Phys B 1970;16:77–84.
[95] STAR Collaboration, Leung YH, et al. Recent hypernuclei measurements in the high baryon density region with the STAR experiment at RHIC. Acta Phys Polon Supp 2023;16:150.
[96] E864 Collaboration, Armstrong TA, et al. Production of $^{3}_{\Lambda}$H and $^{4}_{\Lambda}$H in central 11.5-GeV/c Au + Pt heavy ion collisions. Phys Rev C 2004;70:024902.
[97] A1 Collaboration, Eckert P, et al. Preparation of the hypertriton binding energy measurement at MAMI. PoS 2022;PANIC2021:201.
[98] Nakagawa M, Kasagi A, Liu E, et al. Unique approach for precise determination of binding energies of hypernuclei with nuclear emulsion and machine learning. EPJ Web Conf 2022;271:11006.
[99] Akaishi T, Asano H, Chen X, et al. Precise lifetime measurement of $^{4}_{\Lambda}$H hypernucleus using in-flight $^{4}\mathrm{He}(K^-, \pi^0)^{4}_{\Lambda}\mathrm{H}$ reaction. Phys Lett B 2023;845:138128.
[100] Akaishi T. Experimental status toward the direct lifetime measurement of Hypertriton using the (K^-, π^0) reaction at J-PARC. PoS 2022;PANIC2021:214.

Jinhui Chen is a professor in Physics, working at Institute of Modern Physics of Fudan University. He received his Ph.D. degree from University of Chinese Academy of Sciences in 2008. His recent research focuses on the high energy nuclear collisions.

Xin Dong is a senior scientist, working at Nuclear Science Division of Lawrence Berkeley National Laboratory. He received his Ph.D. degree from University of Science and Technology of China in 2005. His research focuses on the high energy nuclear collisions.

Yugang Ma is a professor in Physics, working at Institute of Modern Physics of Fudan University. He is Academician of the Chinese Academy of Sciences, and Fellow of the American Physical Society. His current research field includes heavy ion physics, laser-nuclear physics, and photonuclear physics etc.

Zhangbu Xu is Distinguished Scientist at Brookhaven National Laboratory, USA, and Fellow of the American Physics Society. He received his Ph.D. degree from Yale University in 1999. His research focuses on high-energy nuclear physics.